New constraints on the rupture process of the 1999 August 17 Izmit earthquake deduced from estimates of stress glut rate moments

G Clévédé, G Bouin, G Bukchin, G Mostinskiy, G Patau

Geophys. J. Int. (2004) **159,** 931–942 doi: 10.1111/j.1365-246X.2004.02304.x

New constraints on the rupture process of the 1999 August 17 Izmit earthquake deduced from estimates of stress glut rate moments

E. Clévédé,[1] M.-P. Bouin,[1] B. Bukchin,[2] A. Mostinskiy[2] and G. Patau[1]

[1] *Département de Sismologie, UMR* 7580, *Institut de Physique du Globe de Paris, France. E-mail: clevede@ipgp.jussieu.fr*
[2] *International Institute for Earthquake Prediction Theory and Mathematical Geophysics, Moscow, Russian Federation*

Accepted 2004 February 27. Received 2004 February 18; in original form 2003 May 6

SUMMARY

This paper illustrates the use of integral estimates given by the stress glut rate moments of total degree 2 for constraining the rupture scenario of a large earthquake in the particular case of the 1999 Izmit mainshock. We determine the integral estimates of the geometry, source duration and rupture propagation given by the stress glut rate moments of total degree 2 by inverting long-period surface wave (LPSW) amplitude spectra. Kinematic and static models of the Izmit earthquake published in the literature are quite different from one another. In order to extract the characteristic features of this event, we calculate the same integral estimates directly from those models and compare them with those deduced from our inversion. While the equivalent rupture zone and the eastward directivity are consistent among all models, the LPSW solution displays a strong unilateral character of the rupture associated with a short rupture duration that is not compatible with the solutions deduced from the published models. With the aim of understand this discrepancy, we use simple equivalent kinematic models to reproduce the integral estimates of the considered rupture processes (including ours) by adjusting a few free parameters controlling the western and eastern parts of the rupture. We show that the joint analysis of the LPSW solution and source tomographies allows us to elucidate the scattering of source processes published for this earthquake and to discriminate between the models. Our results strongly suggest that (1) there was significant moment released on the eastern segment of the activated fault system during the Izmit earthquake; (2) the apparent rupture velocity decreases on this segment.

Key words: earthquake kinematics, integral estimates, rupture process, stress glut rate moments.

1 INTRODUCTION

The determination of the spatial and temporal distribution of slip over the fault area of large earthquakes is an important seismic goal for understanding the mechanics of the seismic rupture and its environmental impact.

Nowadays, when large earthquakes occur in sensitive areas, numerous studies provide source tomographies. These works, based on different types of data and/or different methodological approaches, lead to models of the rupture process that are often different.

This is the case for the devastating $M_w = 7.4$ Izmit earthquake that occurred in Turkey on 1999 August 17. This earthquake ruptured a splay connecting the Marmara Sea pull-apart, along the northern branch of the North Anatolian Fault. The surface rupture runs nearly east–west and extends over at least 120 km (see Fig. 1) (Armijo *et al.* 2000). Surface slip is almost pure right-lateral strike-slip (Barka *et al.* 2002). The geometry of the aftershock area coincides well with the distribution of the observed surface breakage and extends over a depth of 20 km (Özalaybey *et al.* 2002). The location of the epicentre clearly indicates bilateral rupture propagation. A wide variety of data were available for this event, covering the whole spectrum of possible observations: tectonic data as fault geometry and coseismic surface offset, geodetic data including GPS measurements, synthetic aperture radar interferometry (InSAR) and SPOT images and seismological data from teleseismic waves to near-field strong motions. Inversion of these data, independently or combined, provides several source tomographies (Yagi & Kikuchi 2000; Delouis *et al.* 2000; Reilinger *et al.* 2000; Wright *et al.* 2000; Michel & Avouac 2002; Bouchon *et al.* 2002; Sekiguchi & Iwata 2002; Li *et al.* 2002; Feigl *et al.* 2002; Çakir *et al.* 2003; Vallée and Bouchon 2004).

In this paper our aim is to understand the meaning of the differences between those models. To achieve this, we propose to extract the low-frequency information contained in the models.

Backus (1977a,b) pointed out that the low-degree moments of stress glut rate yield information about average rupture extent, duration and velocity of an earthquake. Stress glut rate moments are usually obtained through teleseismic data inversion and yield

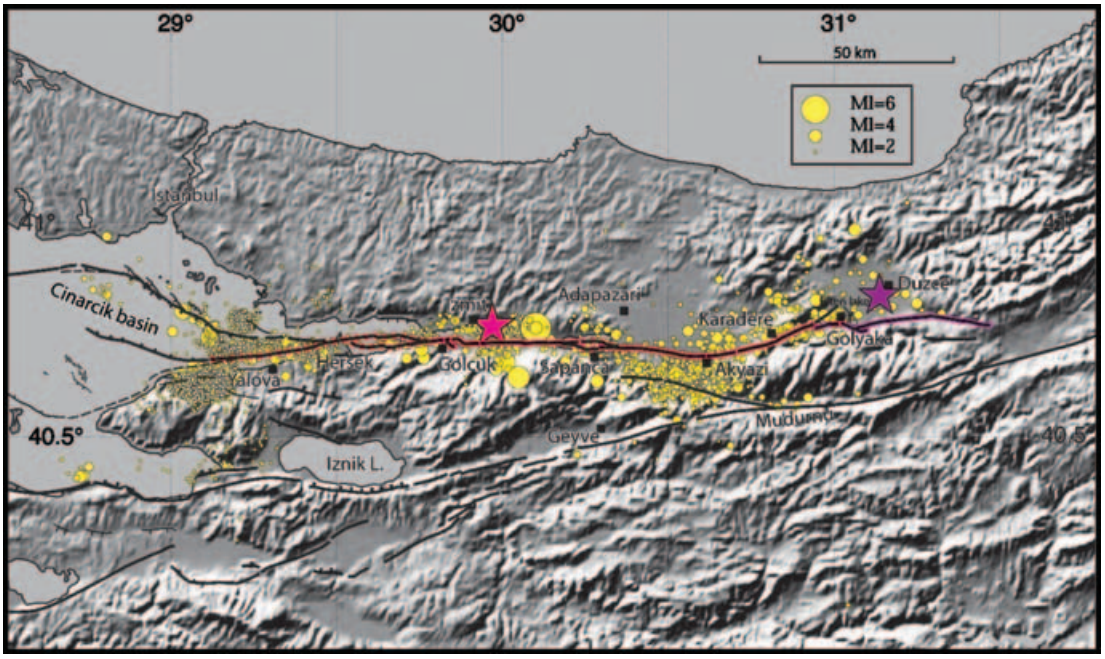

Figure 1. Izmit earthquake region. Breaks of the Izmit (1999 August 17) and Düzce (1999 November 12) events are highlighted in red and purple respectively. Stars denote epicentres of mainshocks. Yellow circles are $M_L \geq 2$ aftershocks recorded between 1999 August 20 and 1999 October 20 by the Tübitak network (Özalaybey *et al.* 2002) and by a temporary array (Karabulut *et al.* 2002). The background DEM image is from GTOPO30. (Figure from Çakir *et al.* (2003).)

integral estimates of the source characteristics. Das & Kostrov (1997) have shown the possibility of using teleseismic body wave records for reconstruction of the integral characteristics of a seismic source. They demonstrated that the Hausdorff constraints can be efficiently used to stabilize the solution of the inverse problem.

A few earthquakes have been studied from this point of view (e.g. Doornbos 1982; Gusev & Pavlov 1988; Bukchin 1995; Gomez *et al.* 1997a,b; Dahm & Krüger 1999; McGuire *et al.* 2000, 2001, 2002). Until now, a direct estimation of the full set of spatiotemporal integral characteristics of the source (corresponding to stress glut rate moments of degree 0, 1 and 2) performed using direct measurements of the slip rate has never been carefully compared with those deduced from inversion. Only McGuire *et al.* (2002) used these integral estimates to show the overall agreement of the predominantly unilateral character of the rupture for a global catalogue of large earthquakes deduced from teleseismic inversions and models based on strong motion data. Hence, the ability of integral estimates to reflect the 'true' rupture process is difficult to assess. This is of particular importance, as these parameters may be useful for constraining more refined source inversions (McGuire *et al.* 2000, 2001).

In the following we shall first analyse the surface wave data for the Izmit earthquake in order to determine the integral parameters characterizing the spatiotemporal behaviour of the source process using the method described by Bukchin (1995). Then we shall calculate the same integral parameters directly from selected source models, using theoretical formulae described in the Appendix (eqs A1 to A13).

We shall use simple equivalent kinematic models in order to reproduce the integral estimates deduced from long-period surface wave amplitude spectra and from the selected models by adjusting a few free parameters. This will allow us to extract the parameters that control the differences between the models, and to propose new constraints on the rupture history of the Izmit earthquake.

2 SURFACE WAVE DATA ANALYSIS

The fundamental modes of Love and Rayleigh waves are retrieved from observed surface wave trains using frequency–time analysis (FTAN) and floating filtering of signals, as described by Lander (1989a) and Levshin *et al.* (1994). Previous works (Gomez *et al.* 1997a,b; Lasserre *et al.* 2001) have shown that in the same bandpass filter, floating-filtered displacement amplitude spectra are smoother than classically filtered ones, thus their inversion is much more stable. We use amplitude spectra in frequency bands where the signal is of a good quality and polarization anomalies (analysed according to the method described by Lander 1989b) are not large.

Observed records are corrected for attenuation and for instrumental response. We then apply an inversion scheme that estimates the stress glut rate moments of total degree 2 from teleseismic surface wave amplitude spectra. Definitions are given in the Appendix; for a complete description of the method see Bukchin (1995).

We calculate surface wave amplitude spectra assuming that the propagation medium has only smooth and weak lateral inhomogeneities. In this case, the surface wave part of the Green's function is determined by the structure near the source and the receiver, by the average phase velocity along the path and by the geometrical spreading (Woodhouse 1974; Babich *et al.* 1976; Levshin 1985; Levshin *et al.* 1989). The surface wave amplitude spectrum for such a model does not depend on the average phase velocity of the wave. Moreover, if lateral heterogeneities are sufficiently smooth, errors in epicentre location do not affect the amplitude spectrum (Bukchin 1990).

2.1 Point source inversion

As a first step we determined the seismic moment tensor in the point source approximation. We selected records of long-period waves from 16 Federation of Digital Seismograph Networks (FDSN)

Table 1. Structure model of the upper 40 km in the source region.

d (km)	V_p (km s^{-1})	V_s (km s^{-1})	ρ (g cm^3)
2.0	4.51	2.61	2.74
2.0	5.02	2.90	2.74
8.0	6.07	3.51	2.74
16.0	6.14	3.54	2.74
4.0	6.59	3.81	3.00
8.0	7.82	4.52	3.00

d is the layer thickness, V_p is the P-wave velocity, V_s is the S-wave velocity and ρ is the density.

stations. The centroid location (latitude 40.702°, longitude 29.987°) and origin time (00:01.39.8 UT) are fixed and correspond to the United States Geological Survey (USGS) solution. Spectra of Love and Rayleigh fundamental modes recorded at 15 and 16 stations respectively are computed in the frequency range 4–10 mHz (250–100 s). In the source region, we used a regional velocity model from Kandilli Observatory (H. Karabulut, personal communication; Table 1) for the upper 40 km and the preliminary reference earth model (PREM) below. Under the receivers, we used the 3SMAC model (Ricard *et al.* 1996) for the crust and the PREM model below the crust. We used the quality factor given by the PREM model for attenuation correction. We imposed a double-couple mechanism. The moment tensor was obtained by joint inversion of amplitude spectra and first arrival polarities at worldwide stations (Lasserre *et al.* 2001).

Our best fitting solution gives a mechanism described by the following values of strike, dip and slip: 267°, 80° and −174° respectively. The best fitting source depth is around 10 km. The estimate of scalar moment is 1.8×10^{20} N m (see Tables 2 and 3 for seismic moment estimates compilation). This result is in very good agreement with the solutions published for this earthquake (see USGS, Harvard and Toksöz *et al.* 1999; Yagi & Kikuchi 2000; Tibi *et al.* 2001).

2.2 Second moments inversion

In order to estimate the duration and the geometry of the source, we used the amplitude spectra of the fundamental modes of Love and Rayleigh waves in the frequency domain 10–20 mHz (100–50 s). Selecting the records, we try to satisfy two conditions: the quality of signal should be good enough and polarization anomalies not too large (<15°), The azimuthal distribution of stations should be homogeneous. We selected 10 Love wave records and 12 Rayleigh wave records from FDSN stations. Their azimuthal distribution is shown in Fig. 2.

We constrain the moment tensor $\boldsymbol{M}$ and the depth to be the values obtained from the point source inversion. We consider the east–west nodal plane as the fault plane. We then determine the six integral estimates of the parameters corresponding to the spatiotemporal stress glut rate moments of total order 2. These parameters are: the source duration (Δt), the instant centroid mean velocity (v_0), the principal axis lengths of the ellipse describing the spatial extent of the source ($l_{\max}$ and $l_{\min}$), the angle between the ellipse major axis and the strike axis (ϕ_l), and the angle between the velocity vector and the strike axis (ϕ_v). The determination is done by a full exploration of the parameter space (Bukchin 1995) (see Appendix for the definitions of parameters and the residual).

Our inversion (Fig. 3 and Table 4) yields a characteristic duration of 15 s and a characteristic source length of 64 km. The minor ellipse axis length, i.e. the characteristic width, is poorly resolved, lying between 0 and 20 km. The instant centroid mean velocity

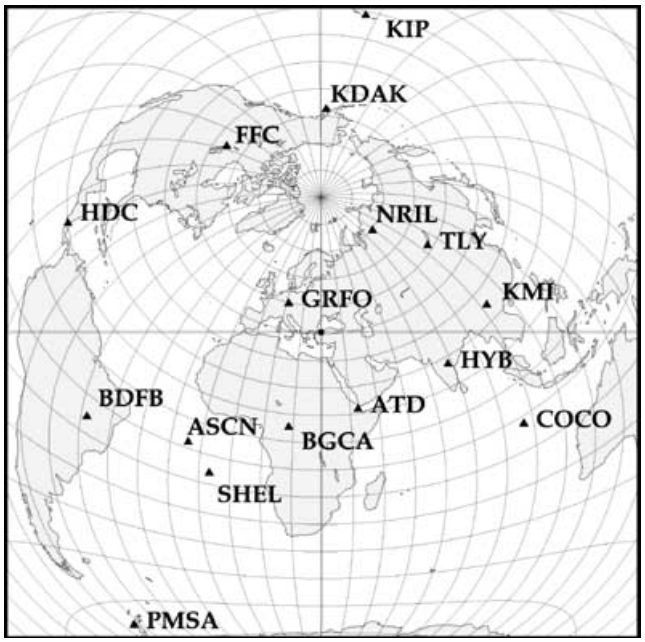

Figure 2. Station distribution used for the second-moments inversion. The figure is centred on the Izmit earthquake hypocentre.

Table 2. Seismic moment estimates: reports. All values in N m.

	Preliminary determination	Updated
USGS	1.4×10^{20}	—
HRV	2.1×10^{20}	2.9×10^{20}
CSEM	2.4×10^{20}	—
PPT	1.8×10^{20}	—

appears to be large, the minimum residual giving a range of 3.6 to 4.2 km s^{-1}.

We fix these parameters to their optimum values and we calculate the residual functions for the angles giving the ellipse and velocity vector orientations. The angles are measured clockwise on the foot wall starting from the strike axis. The results are shown in Fig. 3. Two acceptable solutions are found for both parameters: 25° and 155° for the ellipse orientation and 155° and 205° for the velocity vector orientation. This indetermination is in accordance with the theory and is directly linked to the fact that we use amplitude spectra and to the geometry of the fault: a pure strike-slip on a vertical fault gives rise to two equivalent solutions for both parameters. These orientations are symmetric with respect to the strike axis and it is theoretically impossible to rule out one of the two solutions.

In order to assess the robustness of this solution, we perform different tests. First, we repeat the inversion without constraining the seismic moment. We calculate its value by least-squares minimization of the misfit between the observed and synthetic surface wave amplitude spectra for every current combination of the other parameters (Δt, v_0, $l_{\max}$, $l_{\min}$, ϕ_l and ϕ_v). We obtain a reduction of seismic moment of less than 5 per cent, and estimates for all other parameters do not change.

Second, we consider different centroid depths. The value of the centroid depth obtained from the point source inversion is not well resolved because of the low sensitivity of very long surface wave spectra to relatively small changes in this parameter. Nevertheless, we repeat the second moment inversion for different centroid depths

Table 3. Seismic moment estimates: studies. All values in N m.

	Point source	Finite source	
This study	1.8×10^{20}		Surface waves
McGuire *et al.* (2002)	2.0×10^{20}		Surface waves
Yagi & Kikuchi (2000)	—	1.7×10^{20}	Body waves, strong motions
Tibi *et al.* (2001)	1.4×10^{20}	2.1×10^{20}	Body waves
Bouchon *et al.* (2002)	—	2.6×10^{20}	Strong motions
Sekiguchi & Iwata (2002)	—	1.5×10^{20}	Strong motions
Delouis *et al.* (2000)	—	2.6×10^{20}	InSAR, body waves, strong motions
Çakir *et al.* (2003)	—	1.9×10^{20}	GPS vectors, InSAR, tectonic observations

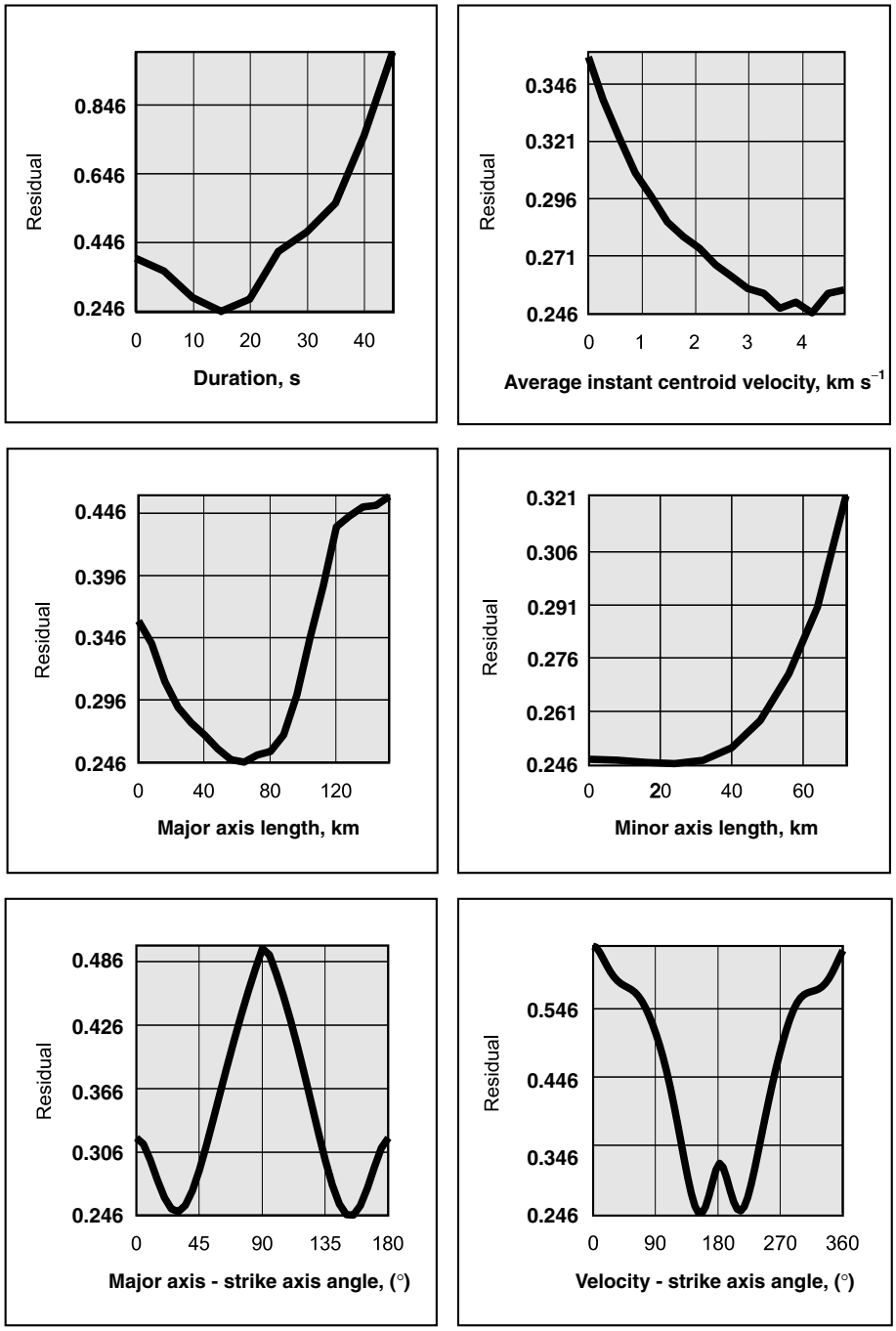

Figure 3. Integral estimates of source characteristics from analysis of 50–100 s surface wave amplitude spectra.

Table 4. Integral characteristics.

	l_{max} (km)	l_{min} (km)	Δt (*s*)	v_0 (km s^{-1})	v_a (km s^{-1})	d
This study	64.0	10.0–20.0	15.0	3.6–4.2	4.27	0.84–0.98
Bouchon *et al.* (2002)	82.8	10.3	11.6	1.65	7.12	0.23
Sekiguchi & Iwata (2002)	67.7	12.5	9.3	1.8	7.24	0.25
Yagi & Kikuchi, (2000)	43.6	10.0	—	—	—	—
Delouis *et al.* (2000)	86.2	9.8	24.3	3.0	3.54	0.85
Çakir *et al.* (2003)	64.7	10.6	—	—	—	—

l_{max}, l_{min}, Δt, v_0 and v_a are, respectively, the major axis length, the minor axis length, the source duration, the instant centroid mean velocity and the apparent rupture velocity, i.e. $l_{max}/\Delta t$. $d = v_0/v_a$ is the directivity ratio as defined in McGuire *et al.* (2002).

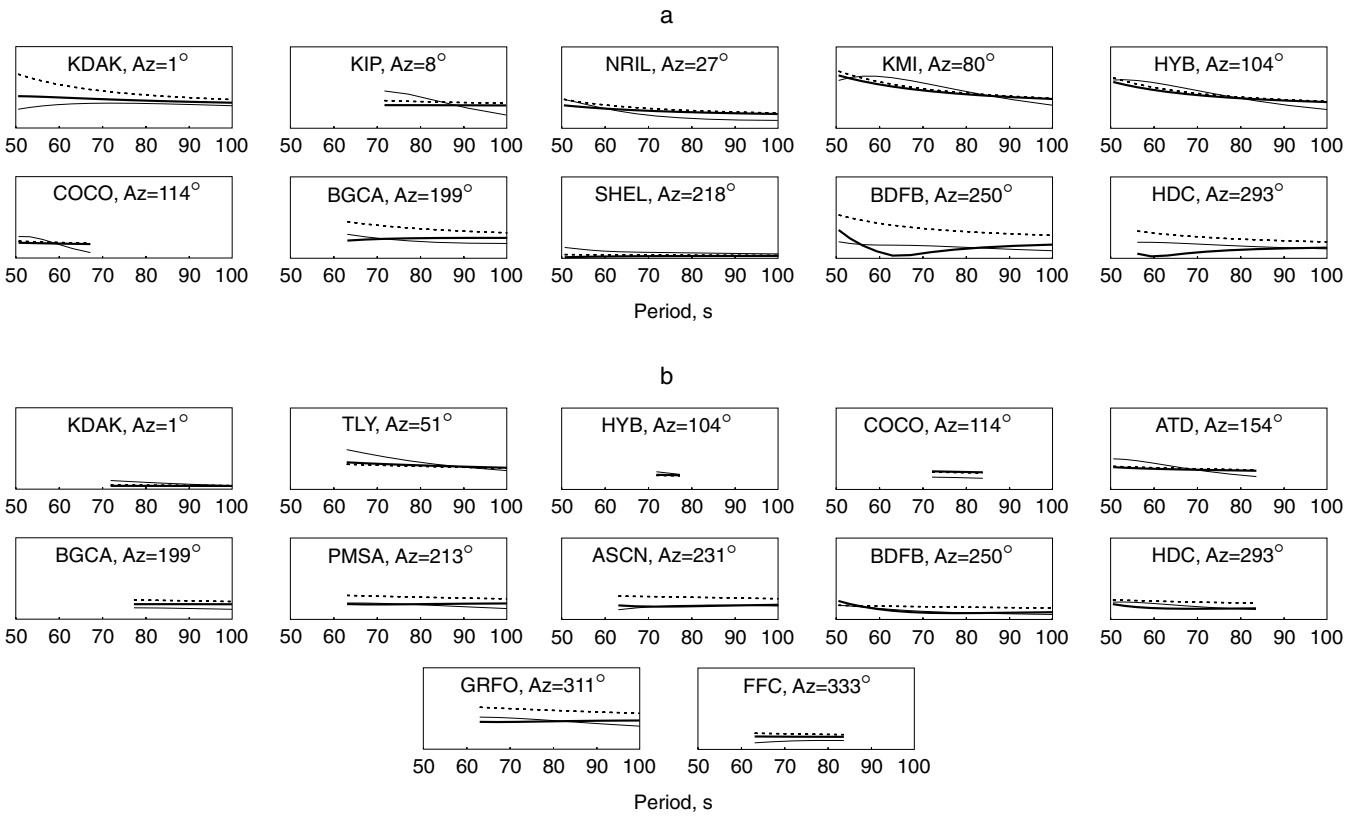

Figure 4. Comparison of observed (thin lines) and synthetic (a) Love and (b) Rayleigh wave amplitude spectra for both moment tensor (dashed lines) and second-moment (thick lines) approximations. All spectra are normalized to the same value.

ranging from 0 to 20 km. The residual functions show little sensitivity to the change of centroid depth, with a minimum around 10 km.

Third, we consider different structural models under the source and receivers. We perform an inversion, choosing the models for receivers from among the four types used by Lasserre *et al.* (2001): the Gutenberg continental model, the oceanic model and two 'tectonic' models with thickened crust. For the source region we used the 3SMAC model (Ricard *et al.* 1996) for the crust and the PREM below the crust. In these cases the minimum of the residual function ($\epsilon(\Delta t, l_{max}, l_{min}, \phi_l, v_0, \phi_v)$ in the Appendix) increased very little, but the optimum values of parameters under estimation did not change.

Finally, we consider the north–south nodal plane as the fault plane. The minimum of the residual function is 32 per cent higher then the value obtained when fixing the east–west plane as the fault plane. This is sufficient to resolve the fault plane ambiguity.

Therefore, regarding these different tests, we consider our solution as stable. In Fig. 4, we compare the observed and synthetic Rayleigh and Love amplitude spectra for both the moment tensor and second moment approximation. Clearly, the spectra computed using the higher-degree moments provide a much better fit of the observed spectra than the simple source model. Our best solution is schematically represented in the top panel of Fig. 6 (see below). The orientations of the source ellipsoid and the instant centroid mean velocity vector are consistent with each other and indicate an eastward propagation of the rupture. This feature of the Izmit earthquake is also clearly displayed in Fig. 5, where we compare the observed Love and Rayleigh surface wave amplitude spectra for the period 77 s with theoretical radiation patterns for both moment tensor and second-moment approximations.

In order to quantify the magnitude of the directivity of the rupture we shall use the directivity ratio d proposed by McGuire *et al.*

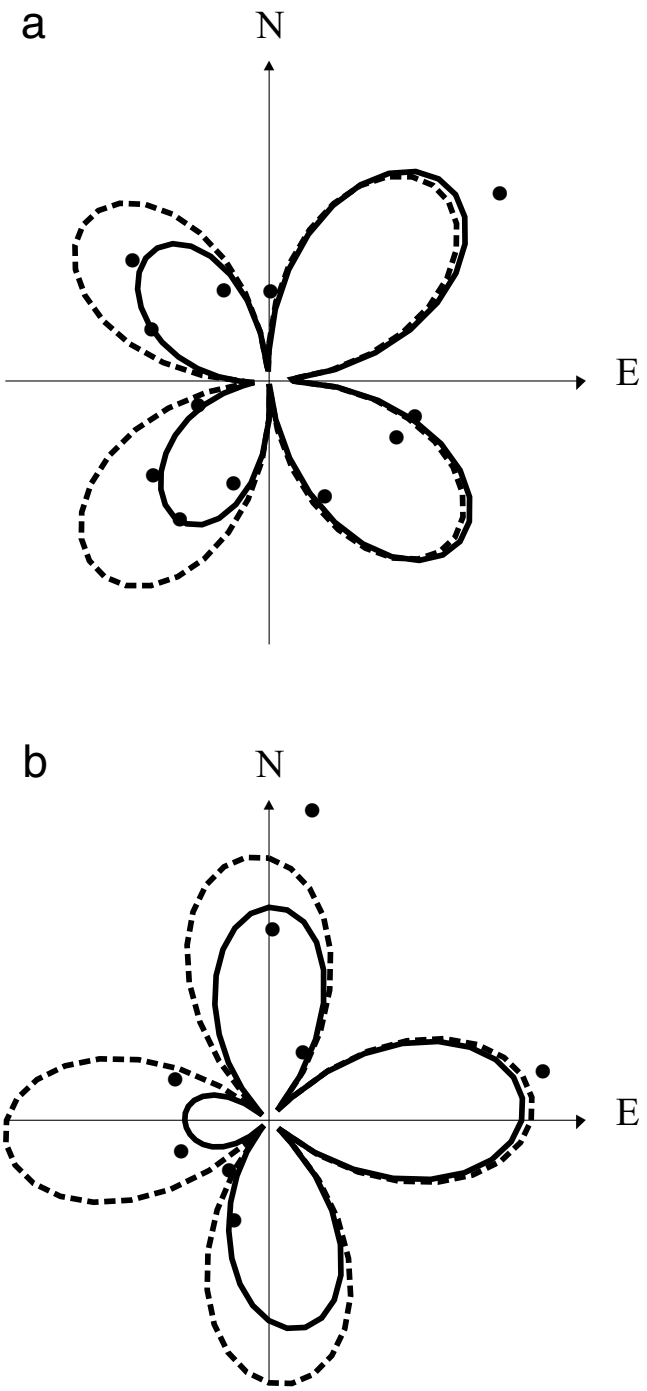

Figure 5. Comparison of observed (dots) and synthetic surface wave amplitude spectra for a period of 77 s for both moment tensor (dashed line) and second-moment approximations (solid line): (a) Rayleigh waves and (b) Love waves. Synthetic amplitude spectra presented in this figure are calculated for an epicentral distance of 9000 km considering the laterally homogeneous model that we used for the source region. Observed amplitude spectra were recalculated for the same epicentral distance and structure.

(2002). This parameter is defined as the ratio between v_0, i.e. the mean velocity vector of the instant centroid (defined in Appendix), and the apparent rupture velocity v_a, that is $l_{max}/\Delta t$. As shown by McGuire *et al.* (2002), for a unilateral rupture where slip nucleates at one end of a rectangular fault and propagates to the other at a rupture velocity v with a uniform slip distribution, $v_a = v_0 = v$. However, for a symmetric bilateral rupture that initiates in the middle and propagates to both ends of a fault at rupture velocity v with uniform slip distribution, $v_a = 2v$ and $v_0 = 0$. Bilateral ruptures correspond to $d = v_0/v_a \leq 1/2$, while predominantly unilateral ruptures correspond to $1/2 < d \leq 1$. Note that this parameter is equivalent to the ratio l_0/l_{max} where l_0 is the characteristic propagation distance defined as $l_0 = v_0\ \Delta t$. We find a value of 0.84 for our model, which is in good agreement with the value of 0.81 obtained by McGuire *et al.* (2002) using a different method. This value suggests a predominantly unilateral rupture.

3 COMPARISON WITH OTHER MODELS

Several groups have published rupture models for the Izmit earthquake, using a wide variety of data. These models appear to be quite different from one another, from the actual fault rupture extension to the distribution of slip patches on the fault plane. In order to compare these models with ours, we propose to compute the integral characteristics corresponding to the stress glut rate moments of degree 0, 1 and 2 of such models directly from their theoretical definitions (see Appendix, eqs A1 to A13).

From the available models we chose five based on different data sets and/or techniques: one is a static model of coseismic slip distribution deduced from InSAR, GPS data and tectonic observations from Çakir *et al.* (2003); three kinematic models, two of them from Bouchon *et al.* (2002) and Sekiguchi & Iwata (2002) based on strong motion data and the third from Delouis *et al.* (2000) obtained from joint inversion of InSAR, teleseismic body wave and strong motion data; we also use the static part of the model of Yagi & Kikuchi (2000) deduced from joint inversion of teleseismic body waves and strong motion data. Kinematic information is unfortunately not available for this model. The spatial slip distributions for these models are presented in Fig. 6 (the rupture times and rise times of the kinematics models are not shown here).

3.1 Integral parameters of source tomographies

For these five models we compute the scalar seismic moment, the spatial centroid location and the ellipse characteristics (principal axis lengths and orientation). For the three kinematic models we also compute the temporal centroid, the integral estimate of the source duration, the instant centroid mean velocity vector and the directivity ratio. The results are summarized in Table 4 and Fig. 6.

A remarkable feature displayed in Fig. 6 and Table 4 is the consistency of the source dimension (given by the length of the major and minor axis of the ellipse): on one hand between the one deduced by the surface wave inversion and those deduced *a posteriori* by applying theoretical formulae using the slip distributions given by the models; and on the other hand between the models discussed, except for that of Yagi & Kikuchi (2000). This suggests that despite the wide variability displayed by the models the spatial degree-2 moment estimate is a robust parameter for estimating the size of the rupture dimension; and this parameter is well resolved for this earthquake by long-period surface wave analysis.

Further, the instant centroid mean velocity vector obtained from our inversion of long-period surface waves indicates a directivity effect toward the east in agreement with the velocity vectors calculated from the kinematic models.

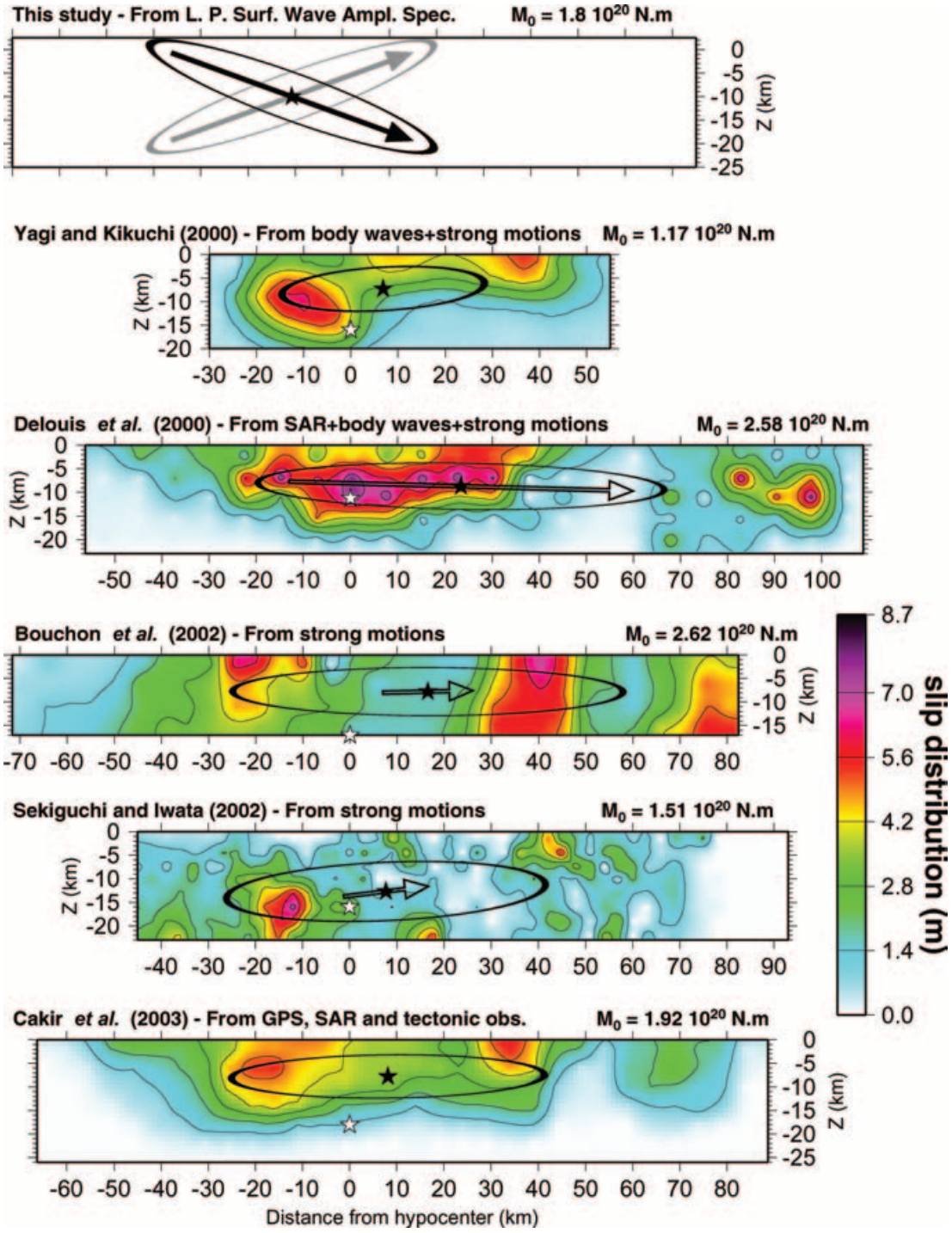

Figure 6. Spatial slip distribution and integral characteristics for kinematic and static models plotted on the assumed fault plane. West is to the left and east is to the right. Grey stars indicate the nucleation point for the kinematic models. Black stars indicate the spatial centroid location. Ellipses represent the second spatial moment. Arrows represent the mean centroid velocity vectors obtained for the kinematic models scaled to the characteristic propagation distance $v_0 \Delta t$. The spatial scales respect the aspect figure of the fault plane grids. Both spatial and slip distribution scales are identical for the five models. Top: scheme of source parameters for the best-fitting solution. Note that the two equivalent solutions symmetric with respect to the strike axis are represented.

However, some rupture parameters display strong discrepancy between the different models. The source duration deduced from surface wave inversion is comparable to that deduced from the models of Bouchon *et al.* (2002); Sekiguchi & Iwata (2002), but the model of Delouis *et al.* (2000) gives a significantly higher value for the source duration (around 10 s longer than ours).

The directivity ratio deduced from our model is in agreement with that deduced from the model of Delouis *et al.* (2000). Both are characterized by a predominantly unilateral rupture towards the east. Conversely, the models of Bouchon *et al.* (2002) and Sekiguchi & Iwata (2002) show a bilateral rupture with a directivity to the east. Hence, our model combines a rather 'short' source time duration

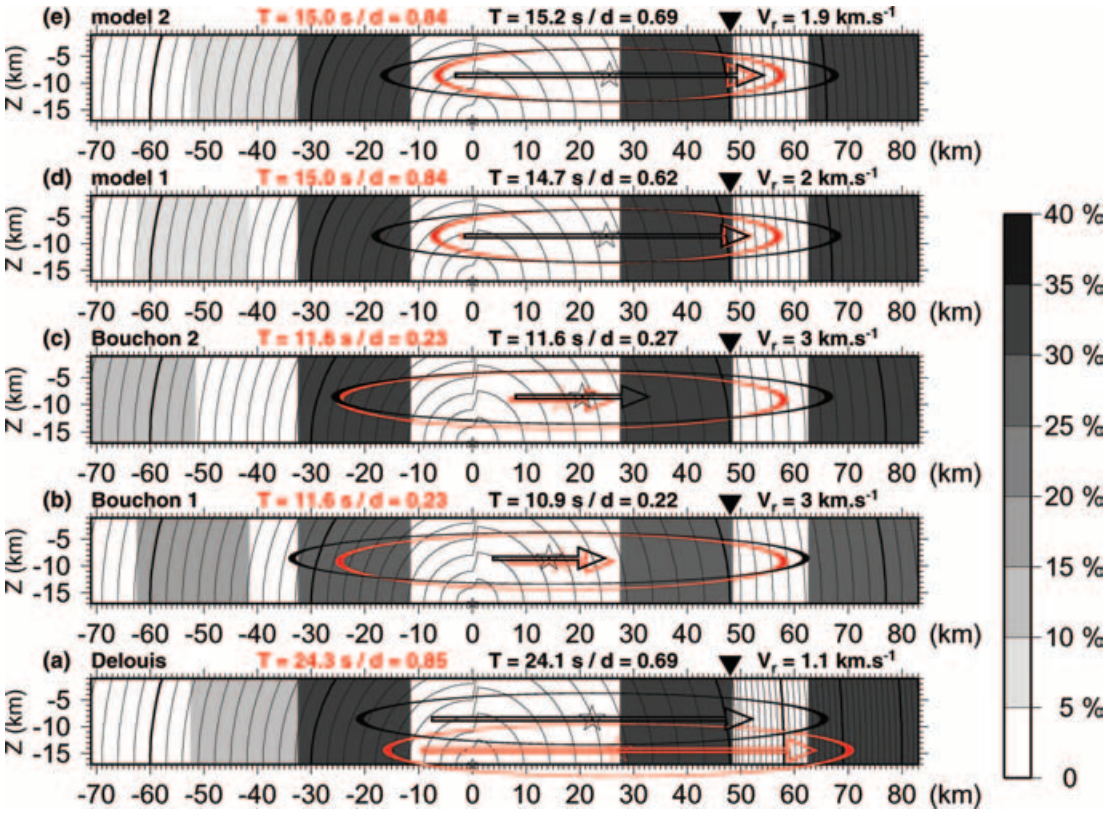

Figure 7. Equivalent models. Spatial slip distribution on the assumed fault plane is expressed in percentage of the total seismic moment. West is to the left and east is to the right. We superimpose the rupture time (every 1 s). White stars indicate the hypocentre of the equivalent models. Stars indicate the spatial centroid location. Ellipses represent the second spatial moment. Arrows represent the mean centroid velocity vectors scaled to the characteristic propagation distance $v_0\ \Delta t$. Black stars, ellipses and arrows are calculated from the equivalent models. Red stars, ellipses and arrows are calculated from the reference models. Respectively from bottom to top: (a) Delouis *et al.* (2000), (b, c) Bouchon *et al.* (2002), (d, e) this study. Source duration estimate and directivity ratio are recalled in red for the reference models and are given in black for the equivalent models together with the rupture velocity on the last east segment (from the position indicated by the black triangle to the eastern end).

and a strong unilateral character, which does not seem compatible with the other kinematic models.

3.2 Equivalent models

In order to understand this apparent discrepancy, we shall try to isolate the features that allow us, for the same class of model, to control at the same time the duration and the directivity, conserving the characteristics that appear robust in all the models. To do so, we shall use simple kinematic models, equivalent in terms of integral parameters. In order to avoid any possible trade-off between the kinematic parameters, we choose to consider (1) areas of uniform slip distribution isolated on the fault plane, and null slip elsewhere, and (2) segments of uniform rupture velocity. To build these equivalent models, we need to fix a maximum number of parameters. We shall extract the robust parameters shared by all the models.

First of all, all the models plotted in Fig. 6 and other models published in the literature (Li *et al.* 2002; Vallée and Bouchon 2004) share a similar feature: most of the energy release occurs in the central part of the activated fault plane. Two main sources of slip can be identified (except for Delouis *et al.* 2000), one is centred between 10 and 20 km west of the epicentre, the other between 35 and 40 km east of the epicentre. We then shall fix two sources of slip on the central segments, one patch laying between 10 and 30 km west of the hypocentre, the other one lying between 30 and 50 km east of the hypocentre. The relative corresponding seismic moment is more scattered than the location but we shall consider that the two sources have the same seismic moment.

Another point that appears robust is the dimension of the fault plane, mainly 140 km long by 20 km wide, except for Yagi & Kikuchi (2000). For practical purposes we shall consider the fault dimension and hypocentre location of Bouchon *et al.* (2002). Note that the vertical extension of the theoretical fault plane has no effect, as the model can be seen as unidimensional.

The fault plane is divided in four segments, two to the west of the hypocentre location and two to the east. The two central segments are delimited by the western and eastern edges of the west and east main slip patches respectively (see Fig. 7).

Then we shall fix the kinematics. Of the three kinematic models plotted in Fig. 6, two (Bouchon *et al.* 2002; Sekiguchi & Iwata 2002) of them present a super shear rupture velocity between the hypocentre and the east main source of slip. Elsewhere the rupture velocity is subshear and is about 3 km s^{-1}. These models are based on strong motions, which are the data set that contains the most information about the timing of the rupture process. In particular the occurrence of super shear rupture velocity to the east has been clearly demonstrated by Bouchon *et al.* (2001). We shall then consider constant rupture velocities fixed at 4.8 km s^{-1} between the hypocentre and the end of the central eastern segment, and 3 km s^{-1} on the western segments.

All these fixed elements constitute the core of the equivalent model. Other less constrained aspects of the rupture have to be

considered. The extension of the rupture to the west up to 65 km from the epicentre is now well established by results deduced from different and independent data sets. Indeed GPS (Reilinger *et al.* 2000), interferometry (Wright *et al.* 2000; Çakir *et al.* 2003) and strong motion data (Bouchon *et al.* 2002) require that slip gradually dies off from the western main source to 50 km west, in good agreement with the aftershock activity recorded on this segment (Karabulut *et al.* 2002). Moreover, a fresh rupture trace of about 1.5 m was observed at 40 km from epicentre during the Marmara Scarp experiment in 2002 September (A. Armijo, personal communication).

Slip in the eastern part of the fault (from 60 km east to hypocentre) is less well constrained and more dependent on the studies. That slip occurred between 60 and 100 km from epicentre during the Izmit earthquake is required by field and GPS data: a coseismic right lateral slip up to 1.5 m has been measured on this segment (Barka *et al.* 2002) and a displacement of 1.3 m was recorded by a GPS station close to the fault (Reilinger *et al.* 2000). The closest strong motion station (DZC) is located in the city of Düzce, 20 km east beyond the eastern termination of the rupture. It is an analogue station without a pre-trigger time and no absolute time. The records miss the *P* arrival. Thus this station cannot be used without making some assumptions. In any case the large amplitude of horizontal velocities (60 cm s^{-1}) recorded at this station requires consequent slip on the eastern segment.

Both Bouchon *et al.* (2002) and Delouis *et al.* (2000) used the strong motion recorded at this station to constrain the slip history on the eastern segment but with different assumptions for the triggering. Sekiguchi & Iwata (2002) withdrew this station from their inversion process and, thus, did not resolve the slip distribution on this part of the fault plane.

Hence, we choose the variable parameters of our model as follows: (1) the seismic moment and location of the slip area on the western segment and (2) the seismic moment and the rupture velocity on the eastern segment. In this comparison, we discard the model of Yagi & Kikuchi (2000) because the fault size is restricted to the central segments of the rupture, and the model of Sekiguchi & Iwata (2002) because it does not contain slip on the eastern segment. Hereafter we shall refer to the models of Delouis *et al.* (2000) and Bouchon *et al.* (2002) and to our study as the reference models.

We perform an exploration of the free parameter space and select the models that give the best fit in terms of source duration estimate and directivity ratio v_0/v_a for the reference models. The validity of the equivalent model is also assessed *a posteriori* by considering the other integral estimates (size of the ellipse axis, instant centroid mean velocity vector). Results are summarized in Fig. 7. On the fault plane representation we plot in black the spatial centroid (star), the second spatial moment (ellipse) and the mean centroid velocity vector scaled to the characteristic propagation distance $v_0\Delta t$ (arrow) calculated from the equivalent models. In order to help the comparison, we superimpose in red the corresponding parameters calculated from the reference models (Fig. 7). Because of the simplicity of the equivalent models, we shall not consider here the orientations of the major axis of the ellipse or of the mean centroid velocity vector. The position of the red ellipses in Fig. 7 respects the relative distance of the spatial centroid to the hypocentre of the reference model considered (Fig. 6).

4 DISCUSSION

In order to illustrate the sensitivity of the integral characteristics with respect to the free parameters of the model, we will present different equivalent models for each reference model: in the case of Bouchon *et al.* (2002), the two models display the trade-off between the location of the western slip patch and its seismic moment; in the case of Delouis *et al.* (2000), when imposing non-null slip on the western segment only the model displayed satisfies the terms of the integral characteristics; in the case of the long-period surface wave solution, we show two possible equivalent models with different location of the western patch. As illustrated, the closer the western patch is to the hypocentre, the higher is the directivity ratio. We found that an acceptable upper bound for the amount of slip on the western segment corresponds to about 5 per cent of the total seismic moment, which is compatible with the models of Bouchon *et al.* (2002) and Delouis *et al.* (2000). However, the principal feature is that a consequent amount of slip, around 30per cent of the total of the seismic moment, is required on the eastern segment for both models. Again, such a feature is shared with the models of Bouchon *et al.* (2002) and Delouis *et al.* (2000).

Hence, the equivalent models are consistent in terms of slip distribution along the fault. The most striking discrepancy is the timing of the rupture on the eastern segment. Comparison between models clearly indicates that the average rupture velocity on the eastern segment controls both the source duration and the directivity ratio. The smaller the rupture velocity, the higher the source duration and the directivity ratio.

From this point of view, the long-period surface wave solution, characterized by a rather 'short' source duration and a high directivity ratio, appears to lie in between that of Bouchon *et al.* (2002) ('short' source duration and small directivity ratio) and Delouis *et al.* (2000) ('long' source duration and high directivity ratio). The comparison between model (a) and model (e) in Fig. 7, displaying comparable slip distribution and giving the same directivity ratio, clearly demonstrates that the source duration is directly sensitive to the kinematics on the eastern segment. In order to obtain a source duration close to the one deduced from the long-period surface wave inversion (15 s), and to keep a qualitative agreement for the directivity ratio, we find a lower bound value for the average rupture velocity on the eastern segment of 1.9 km s^{-1}.

In the light of this analysis we shall now propose an interpretation of the results obtained from the long-period surface wave inversion in terms of rupture process for the Izmit earthquake. Assuming that most of the energy was released on the central part of the activated fault, from Gölcük to Akyazi, our results suggest that:

(1) There was a strong moment release on the eastern segment, about 30 per cent of the total seismic moment. This slip must be deep to be consistent with the coseismic measured surface offset (up to 1.5 m) and the GPS displacement at Karadere. Such a high slip on the eastern segment is in agreement with most of the seismological studies (Bouchon *et al.* 2002; Delouis *et al.* 2000; Li *et al.* 2002). The apparent inconsistency with the static models (Reilinger *et al.* 2000; Wright *et al.* 2000; Feigl *et al.* 2002; Çakir *et al.* 2003) can be explained by the poor quality of the SAR data in the eastern part of the fault region together with the lack of resolution in depth of geodetic data in the particular case of a vertical fault (Hernandez *et al.* 1999). Indeed, a deep slip source on the eastern segment is compatible with InSAR and GPS data (Z. Çakir, personal communication).

(2) The slip on the western segment has to be low, less than 10 per cent of the total seismic moment. This amount of slip is consistent between all the models (e.g. Reilinger *et al.* 2000; Wright *et al.* 2000; Feigl *et al.* 2002; Çakir *et al.* 2003; Bouchon *et al.* 2002;

Delouis *et al.* 2000; Li *et al.* 2002), regardless of the type of data used, and then appears to be reliable.

Assuming a supershear rupture velocity on the central east segment, our results suggest that:

(3) The apparent rupture velocity decreased significantly on the eastern segment down to about 1.9 km s^{-1}. Bouchon *et al.* (2002) demonstrated that the records at DZC required the average rupture velocity on this segment to be 3 km s^{-1}. The corresponding time of rupture propagation in this case is about 6 s longer than for a velocity of 1.9 km s^{-1}. Then, assuming the rupture velocity on the eastern segment to be 3 km s^{-1}, we propose that the rupture stopped on the intersegment between Akyazi and Karadere, where no coseismic surface slip has been observed (Barka *et al.* 2002) and where the fault changes strike (see Fig. 1), and delayed the rupture on the last eastern segment by up to 6 s. This hypothesis is mechanically more consistent than an energy release together with a rupture deceleration.

The Bouchon *et al.* (2002) model is not inconsistent with such a hypothesis. Indeed the published model (Bouchon *et al.* 2002) is obtained assuming the earliest possibility for the triggering time of DZC. In other words, this model is the fastest in terms of apparent rupture velocity. The latest estimate of triggering, 4.2 s later (Bouchon *et al.* 2000), leads to a slower apparent rupture velocity, within the range of values we found.

It is important to note that slowing down the rupture to subshear values on the central eastern segment will result in a decrease of the time delay down to zero.

Two studies (Delouis *et al.* 2000; Li *et al.* 2002) propose that significant energy was released up to 50 s on the eastern segment. Such a rupture duration is not compatible with the long-period surface wave data.

5 CONCLUSION

We use analysis of surface wave amplitude spectra to retrieve the total degree-2 stress glut rate moments describing the low-frequency spatiotemporal source behavior of the 1999 Izmit earthquake. We compare our results with those deduced from source tomographies based on different data sets. To do this, we calculate directly the integral characteristics of the source using the theoretical formulation, applied to these models. In order to understand the inconsistencies between the models, we use simple equivalent kinematic models to reproduce the integral estimates of the rupture processes by adjusting a few free parameters. The simple model design shows a good ability to provide equivalent models in terms of integral estimates of the rupture in all the cases. We show that the amount of seismic moment released and the kinematics on the eastern segment, the less well constrained part of the rupture, control the discrepancy between the source tomographies. We demonstrate that analysis of the long-period surface wave amplitude spectra strongly supports the hypothesis of a strong moment release together with a decrease in the average rupture velocity on the eastern segment.

We point out that not only is determination of integral estimates from long-period surface wave amplitude spectra relevant to constrain some aspects of the rupture process, but also that determination of integral estimates from source tomographies is pertinent as it provides an objective tool for model intercomparison. Moreover we show that a joint analysis is a powerful approach for assessing the resolution limits of the models and to discriminate between them.

ACKNOWLEDGMENTS

We thank Michel Bouchon, Ziyadine Çakir, Haruko Sekiguchi, Yaji Yagi and Bertrand Delouis for providing us with their models. We are very grateful to J. McGuire and F. Krüger for their helpful comments on an earlier version of this paper. This paper has benefited from fruitful discussions with Pascal Bernard, Zyanedine Çakir and Jean-Bernard de Chabalier. This research was supported by the Institut Universitaire de France, while B. Bukchin and A. Mostinskiy visited the IPGP. B. Bukchin also acknowledge support from the International Science and Technology Center, project 1293–99, and NATO Grant SfP—97226. This is IPGP contribution no 1991.

REFERENCES

Armijo, A., Meyer, B., Barka, A., de Chabalier, J.-B. & Hubert, A., 2000. The fault breaks of the 1999 earthquakes in Turkey and the tectonic evolution of the sea of Marmara: a summary, in, *The Izmit and Düzce earthquakes: Preliminary Results*, pp. 55–62, ed. Barka, A., ITU, Istanbul, Turkey.

Backus, G.E., 1977a. Interpreting the seismic glut moment of total degree 2 or less, *Geophys. J. R. astr. Soc.,* **51,** 1–25.

Backus, G.E., 1977b. Seismic source with observable glut moment of spatial degree two, *Geophys. J. R. astr. Soc.,* **51,** 27–45.

Babich, V.M., Chikachev, B.A. & Yanovskaya, T.B., 1976. Surface waves in a vertically inhomogeneous elastic half-space with weak horizontal inhomogeneity, *Izv. Akad. Nauk SSSR, Fiz. Zemli,* **4,** 24–31.

Barka, A. *et al.,* 2002. The surface rupture and slip distribution of the 17 August 1999 Izmit earthquake (M 7.4), North Anatolian Fault, *Bull. seism. Soc. Am.,* **92**(1), 43–60.

Bouchon, M., Toksöz, N., Karabulut, H., Bouin, M.P., Dietrich, M., Aktar, M. & Edie, M., 2000. Seismic imaging of the Izmit rupture inferred from the near-fault recordings, *Geophys. Res. Lett.,* **27**(18), 3013–3016.

Bouchon, M., Bouin, M.-P., Karabulut, H., Toksöz, N., Dietrich, M. & Rosakis, A.J., 2001. How fast is rupture during an earthquake? New insights from the 1999 Turkey earthquakes, *Geophys. Res. Lett.,* **28**(14), 2723–2725.

Bouchon, M., Toksöz, N., Karabulut, H., Bouin, M.P., Dietrich, M., Aktar, M. & Edie, M., 2002. Space and time evolution of rupture and faulting during the 1999 Izmit (Turkey) earthquake, *Bull. seism. Soc. Am.,* **92**(1), 256–266.

Bukchin, B.G., 1990. Determination of source parameters from surface wave recordings allowing for uncertainties in the properties of the medium, *Izv. Akad. Nauk SSSR, Fiz. Zemli,* **25,** 723–728.

Bukchin, B., 1995. Determination of stress glut moments of total degree 2 from teleseismic surface wave amplitude spectra, *Tectonophysics,* 185–191.

Çakir, Z., de Chabalier, J.-B., Armijo, A., Meyer, B., Barka, A. & Peltzer, G., 2001. The August 17, 1999 Turkey earthquake seen with InSAR imagery and tectonic field observations, *EUG XI Meeting, 8–12 April 2001*, *Strasbourg*, *France*, p. 295, Cambridge Publications.

Çakir, Z., de Chabalier, J.B., Armijo, R., Meyer, B., Barka, A. & Peltzer, G., 2003. Coseismic and early postseismic slip associated with the 1999 Izmit earthquake (Turkey), from SAR interferometry and tectonic field observations, *Geophys. J. Int.*, **155,** 93–110.

Dahm, T. & Krüger, F., 1999. Higher-degree moment tensor inversion using far-field broad-band recordings: theory and evaluation of the method with application to the 1994 Bolivia deep earthquake, *Geophys. J. Int.,* **137**, 35–50.

Das, S. & Kostrov, B.V., 1997. Determination of the polynomial moments of the seismic moment rate density distributions with positivity constraints, *Geophys. J. Int.,* **131,** 115–126.

Delouis, B., Lundgren, P., Salichon, J. & Giardini, D., 2000. Joint inversion of InSAR and teleseismic data for the slip history of the 1999 Izmit (Turkey) earthquake, *Geophys. Res. Lett.,* **27**(20), 3389–3392.

Doornbos, D.J., 1982. Seismic moment tensors and kinematic source parameters, *Geophys. J. R. astr. Soc.,* **69,** 235–251.
Feigl, K. L. *et al.,* 2002. Estimating slip distribution for the Izmit mainshock from coseismic GPS, RADARSAT, ERS-1, and SPOT measurements, *Bull. seism. Soc. Am.,* **92,** 138–160.
Gomez, J.M., Bukchin, B., Madariaga, R., Rogozhin, E.A. & Bogachkin, B., 1997a. Rupture process of the 19 August 1992 Susamyr, Kyrgyzstan, earthquake, *J. Seismol.,* **1,** 219–235.
Gomez, J.M., Bukchin, B., Madariaga, R. & Rogozhin, E.A., 1997b. A study of the Barisakho, Georgia, earthquake of October 23 1992 from broadband surface and body waves, *Geophys. J. Int.,* **129,** 613–623.
Gusev, A.A. & Pavlov, V.M., 1988. Determination of space-time structure of a deep earthquake source by means of power moments, *Tectonophysics,* **152,** 319–334.
Hernandez, B., Cotton, F. & Campillo, M., 1999. Contribution of radar interferometry to a two-step inversion of the kinematic process of the 1992 Landers earthquake, *J. geophys. Res.,* **104**, 13 083–13 099.
Karabulut, H., Bouin, M.-P., Bouchon, M., Dietrich, M., Cornou, C. & Aktar, M., 2002. The seismicity in the eastern Marmara Sea after the 17 August 1999 Izmit earthquake, *Bull. seism. Soc. Am.,* **92,** 387–393.
Lander, A., 1989a. Frequency-time analysis, in *Seismic Surface Waves in Laterally Inhomogeneous Earth,* pp. 153–163, ed. Keilis-Borok, V., Kluwer Academic Publishers, Dordrecht.
Lander, A., 1989b. Linear-polarization analysis, in *Seismic Surface Waves in Laterally Inhomogeneous Earth,* pp. 164–178, ed. Keilis-Borok, V., Kluwer Academic Publishers, Dordrecht.
Lasserre, C., Bukchin, B., Bernard, P., Tapponnier, P., Gaudemer, Y., Mostinskiy, A. & Dailu, R., 2001. Sources parameters and tectonic origin of the 1996 June 1 Tianzhu (M_w = 5.2) and 1995 July 21 Yongden (M_w = 5.6) earthquakes near the Haiyuan fault (Gansu, China), *Geophys. J. Int.,* **144**(1), 206–220.
Levshin, A.L., 1985. Effects of lateral inhomogeneity on surface wave amplitude measurements, *Ann. Geophys.,* **3**(4), 511–518.
Levshin, A.L., Yanovskaya, T.B., Lander, A.V., Bukchin, B.G., Barmin, M.P., Ratnikova, L.I. & Its, E.N., 1989. Recording, identification and measurement of surface wave parameters, in *Seismic Surface Waves in Laterally Inhomogeneous Earth,* pp. 131–182, ed. Keilis-Borok, V.I., Kluwer Academic Publishers, Dordrecht.
Levshin, A., Ritzwoller, M. & Ratnikova, L., 1994. The nature and cause of polarization anomalies of surface waves crossing northern and central Eurasia, *Geophys. J. Int.,* **117,** 577–591.
Li, X., Cormier, V.F. & Toksöz, M.N., 2002. Complex source process of the 17 August 1999 Izmit, Turkey, earthquake, *Bull. seism. Soc. Am.,* **92,** 267–277.
McGuire, J.J., Zhao, L. & Jordan, T.H., 2000. The rupture dimensions of the 1998 Antarctic earthquake from low frequency waves, *Geophys. Res. Lett.,* **27,** 2305–2308.
McGuire, J.J., Zhao, L. & Jordan, T.H., 2001. Teleseismic inversion for the second-degree moments of earthquake space-time distributions, *Geophys. J. Int.,* **145**(3), 661–678.
McGuire, J.J., Zhao, L. & Jordan, T.H., 2002. Predominance of unilateral rupture for a global catalog of large earthquakes, *Bull. seism. Soc. Am.,* **92,** 3309–3317.
Michel, R. & Avouac, J.-P., 2002. Deformation due to the 17 August 1999 Izmit Turkey earthquake measured from SPOT images, *J. geophys. Res.,* **107**(B4), doi:10.1029/2000JB000102.
Özalaybey, S., Karabulut, H., Ergin, M., Aktar, M. & Bouchon, M., 2001. The 1999 Izmit earthquake sequence in NW-Turkey: seismological aspects, in, *Symposia in Seismotectonics of the North-western Anatolia-Aegean and Recent Turkish Earthquakes,* pp. 78–87, ed. Taymaz, T., ITU, Istanbul, Turkey.
Özalaybey, S., Ergin, M., Aktar, M., Tapirdamaz, C., Biçen, F. & Yöruk, A., 2002. The 1999 Izmit earthquake sequence in Turkey: seismological and tectonic aspects, *Bull. seism. Soc. Am.,* **92,** 376–386.
Reilinger, R.E. *et al.,* 2000. Coseismic and postseismic fault slip for the 17 August 1999 M = 7.5, Izmit, Turkey earthquake, *Science,* **286,** 272–276.
Ricard Y., Nataf, H.-C. & Montagner, J.-P., 1996. The 3SMAC model. Confrontation with seismic data, *J. geophys. Res.,* **101,** 8457–8472.
Sekiguchi, H. & Iwata, T., 2002. Rupture process of the 1999 Koaceli, Turkey, earthquake estimated form strong-motion waveforms, *Bull. seism. Soc. Am.,* **92,** 300–311.
Tibi, R. *et al.,* 2001. Rupture processes of the 1999 August 17 Izmit and November 12 Düzce (Turkey) earthquakes, *Geophys. J. Int.,* **144**(2), F1–F7.
Toksöz, M.N., Reilinger, R.E., Doll, C.D., Barka, A.A. & Yalcin, N., 1999. Izmit (Turkey) earthquake of 17 August 1999: first report., *Seism. Res. Lett.,* **70,** 669–679.
Vallée, M. & Bouchon, M., 2004. Imaging co-seismic rupture in far field by slip patches, *Geophys. J. Int.,* **156,** 615–630.
Woodhouse, J.H., 1974. Surface waves in the laterally varying structure, *Geophys. J. R. astr. Soc.,* **90,** 713–728.
Wright. T., Fielding, E. & Parsons, B., 2000. Triggered slip: observations of the 17 August 1999 Izmit (Turkey) earthquake using radar interferometry, *Geophys. Res. Lett.,* **28,** 1079–1082.
Yagi, Y. & Kikuchi, M., 2000. Source rupture process of the Kocaeli, Turkey, earthquake of August 17, 1999, obtained by joint inversion of near-field data and teleseismic data, *Geophys. Res. Lett.,* **27**(13), 1969–1972.

APPENDIX A

We assume that the time derivatives of stress glut tensor $\dot{\mathbf{\Gamma}}$ can be represented in the form

$$\dot{\mathbf{\Gamma}} = f(\mathbf{x}, t)\mathbf{m} \tag{A1}$$

where $f(\mathbf{x}, t)$, the slip rate times μ, is a non-negative function.

Spatial and temporal integral characteristics of the source can be expressed by corresponding moments of the function $f(\mathbf{x}, t)$. The spatiotemporal moments of $f(\mathbf{x}, t)$ total degree 0, 1 and 2 with respect to position $\mathbf{q}$ and instant of time τ are:

$$f^{(0,0)} = \int_V dV \int_0^\infty f(\mathbf{x}, t)\, dt \tag{A2}$$

$$f_i^{(1,0)}(\mathbf{q}) = \int_V dV \int_0^\infty f(\mathbf{x}, t)\,(x_i - q_i)\, dt \tag{A3}$$

$$f^{(0,1)}(\tau) = \int_V dV \int_0^\infty f(\mathbf{x}, t)\,(t - \tau)\, dt \tag{A4}$$

$$f_i^{(1,1)}(\mathbf{q}, \tau) = \int_V dV \int_0^\infty f(\mathbf{x}, t)\,(x_i - q_i)\,(t - \tau)\, dt \tag{A5}$$

$$f_{ij}^{(2,0)}(\mathbf{q}) = \int_V dV \int_0^\infty f(\mathbf{x}, t)\,(x_i - q_i)\,\left(x_j - q_j\right) dt \tag{A6}$$

$$f^{(0,2)}(\tau) = \int_V dV \int_0^\infty f(\mathbf{x}, t)\,(t - \tau)^2\, dt. \tag{A7}$$

Using theses moments, we define the integral characteristics of the source as follows.

The source location is estimated by the spatial centroid $\mathbf{q}_c$ of the field $f(\mathbf{x}, t)$

$$\mathbf{q}_c = \mathbf{f}^{(1,0)}(\mathbf{0})/M_0 \tag{A8}$$

where $M_0 = f^{(0,0)}$ is the seismic moment.

The temporal centroid τ_c is

$$\tau_c = f^{(0,1)}(0)/M_0. \tag{A9}$$

The source duration Δt is estimated by $2\Delta\tau$ with

$$(\Delta\tau)^2 = f^{(0,2)}(\tau_c)/M_0. \tag{A10}$$

The spatial extent of the source is estimated by the matrix $\mathbf{W}$:

$$\mathbf{W} = \mathbf{f}^{(2,0)}(\mathbf{q}_c)/M_0. \tag{A11}$$

The mean source size in direction $\mathbf{r}$ is estimated by the value $2\,l_r$ defined by the formula

$$l_r^2 = \mathbf{r}^{\mathrm{T}}\mathbf{W}\mathbf{r}. \tag{A12}$$

The source principal axes are directed along the eigenvectors of the matrix $\mathbf{W}$.

The mean velocity $\mathbf{v_0}$ of the instant spatial centroid is estimated as

$$\mathbf{v_0} = \mathbf{f}^{(1,1)}(\mathbf{q}_{\mathrm{c}}, \tau_{\mathrm{c}})\,/f^{(0,2)}. \tag{A13}$$

Let the depth and the moment tensor of the best point source be determined using long-period surface waves. We consider here a plane source. Let the fault plane (one of the two nodal planes) be identified. Setting the spatial and temporal origins in corresponding centroids ($\mathbf{q}_{\mathrm{c}} = \mathbf{0}$, $\tau_{\mathrm{c}} = 0$) we express the surface wave amplitude spectra as a function of six parameters:

(1) Δt, estimate of the source duration.
(2) $l_{\max}$, estimate of the maximal mean size of the source.
(3) ϕ_l, estimate of the angle between the source major axis and the strike axis.
(4) $l_{\min}$, estimate of the minimal mean size of the source.
(5) v_0, estimate of the absolute value of the instant centroid mean velocity $\mathbf{v_0}$.
(6) ϕ_v, the angle between $\mathbf{v_0}$ and the strike axis.

We consider a grid in the space of these six parameters. We calculate the amplitude spectra residual $\epsilon(\Delta t, l_{\max}, l_{\min}, \phi_l, v_0, \phi_v)$ for any current combination of values of varying parameters:

$$\epsilon\,(\Delta t, l_{\max}, l_{\min}, \phi_l, v_0, \phi_v) = \left(\frac{\sum_{i=1}^{N} \epsilon^{(i)2}}{\sum_{i=1}^{N} \left|u_{\mathrm{obs}}^{(i)}(\mathbf{r}, \omega)\right|^2}\right)^{1/2} \tag{A14}$$

where ${u^{(i)}}_{\mathrm{obs}}$ is the observed value of the ith spectrum and $\epsilon^{(i)} = |u_{\mathrm{obs}}^{(i)}| - |u_{\mathrm{calc}}^{(i)}|$ is the residual of the ith observed amplitude spectrum with respect to the theoretical one.

We consider as estimates of parameters the values that minimize ϵ. We search them by a systematic exploration of the six-dimensional parameter space. To characterize the resolution of each of these source integral characteristics, we finally calculate the partial residual function for each parameter. This function is defined as follows: we fix the value of one parameter p, and we search for the minimum value $\epsilon_{\min}$ of the residual ϵ for all possible values of the other parameters. For each value of p we define the residual function $\epsilon_p(p) = \epsilon_{\min}$. We repeat this procedure for all the parameters. These partial residual functions are displayed in Fig. 3.